THE ASTROPHYSICAL JOURNAL, 439:722–729, 1995 February 1

ROSAT OBSERVATIONS OF THE UNUSUAL SUPERNOVA REMNANT CTB 80 CONTAINING THE PULSAR PSR 1951+32

SAMAR SAFI-HARB AND HAKKI ÖGELMAN
Department of Physics, University of Wisconsin–Madison, 1150 University Avenue, Madison, WI 53706
AND
JOHN P. FINLEY
Department of Physics, Purdue University, 1396 Physics Building, West Lafayette, IN 47907
Received 1994 May 23; accepted 1994 August 9

ABSTRACT

The unusual supernova remnant CTB 80, containing the 39.5 ms pulsar PSR 1951+32, has been observed with the Position Sensitive Proportional Counter (PSPC) and the High Resolution Imager (HRI) aboard *ROSAT*. The HRI image, centered on the pulsar, is composed of a bright compact core of $\sim 1'$ radius containing the pulsar and a compact nebula, as well as a diffuse nebula extending $\sim 5'$ eastward of the pulsar. The PSPC allowed us to model the spectra of the point source, the compact nebula and the 5′ diffuse nebula. For a power-law spectrum with photon index $\Gamma \sim 2$ and an interstellar column density of $N_H \sim 3 \times 10^{21}$ cm^{-21}, the derived luminosities are $\sim 2.3 \times 10^{33} d_{2.5}^2$ ergs s^{-1} from the pointlike source, $\sim 3.9 \times 10^{33} d_{2.5}^2$ ergs s^{-1} from the compact nebula, and $\sim 1.8 \times 10^{33} d_{2.5}^2$ ergs s^{-1} from the 5′ diffuse nebula. In addition, the 2° diameter circular field of view of the PSPC reveals a hard emission feature southeast of the pulsar with a conical geometry extending out to the edge of the detector. The spectrum from this region is well described by a two-temperature Raymond-Smith thermal plasma with an average temperature of $\sim 10^7$ K and a luminosity of $\sim 10^{34} d_{2.5}^2$ ergs s^{-1}. Pulsations from the 39.5 ms pulsar, PSR 1951+32, are detected at the 99% confidence level. The implied pulsed fraction is $\sim 35\%$ with a complicated energy-dependent behavior. The compact core and the extended diffuse nebula can be explained as synchrotron radiation from the relativistic pulsar wind confined by the ram pressure of the surrounding inhomogeneous medium. The conelike feature detected southeast of PSR 1951+32 is consistent with emission from an optically thin SNR in the radiative cooling phase of its evolution.

Subject headings: ISM: individual (CTB 80) — pulsars: individual (PSR 1951+32) — supernova remnants — X-rays: ISM

1. INTRODUCTION

PSR 1951+32 is a 39.5 ms pulsar located in the core of the supernova remnant (SNR) CTB 80. Morphological studies of CTB 80 in the radio energy band have led to its classification as a composite-type SNR consisting of a plerionic (i.e., center-filled) component and a shell-like component (Velusamy & Kundu 1974; Velusamy, Kundu, & Becker 1976; Angerhofer et al. 1981; Strom, Angerhofer, & Dickel 1984; Mantovani et al. 1985). The plerion consists of a 10′ by 6′ plateau region with a spectral energy index $\alpha = 0.4$ containing a flat ($\alpha = 0$) compact source of $\sim 30''$ diameter at its western edge. The shell-like component comprises three faint 30′ long radio emission ridges with a steeper index $\alpha = 0.8$ which intersect at the plateau's western edge. The radio emission is linearly polarized over large areas of the compact and extended regions suggesting a Crab-like supernova remnant (Weiler 1985). The discovery in the core of CTB 80 of PSR 1951+32, a very fast pulsar with a period of 39.5 ms and a spin-down age of $\sim 10^5$ yr, amplified the interest in CTB 80 (Kulkarni et al. 1988; Fruchter et al. 1988). Optical observations reveal a ring of nebulosity of angular diameter $\sim 50''$ containing knots coincident with the central radio source. The pulsar is inside the central 1′ core that emits strong [S II], [N II], and [O I] relative to Hα (Angerhofer, Wilson, & Mould 1980; Blair et al. 1984; Hester & Kulkarni 1989; Whitehead, Meaburn, & Clayton 1989). X-ray observations (Wang & Seward 1984; Ögelman & Buccheri 1987; Angelini et al. 1988) show a centrally located point source, coincident with the radio core and surrounded by diffuse emission. The X-ray luminosity in the 0.2–4.0 keV band was estimated by Wang & Seward (1984) using *Einstein* IPC data to be $\sim 0.7 \times 10^{34} d_{2.5}^2$ ergs s^{-1} from the central point source and $\sim 1.5 \times 10^{34} d_{2.5}^2$ ergs s^{-1} from the diffuse component. *EXOSAT* observations yielded a total luminosity in the 0.03–2.4 keV band of $\sim (0.5\text{–}3.2) \times 10^{34} d_{2.5}^2$ ergs s^{-1} under the assumption of a power-law spectrum of photon index $\Gamma = 2$ (Ögelman & Buccheri 1987). Fesen, Shull, & Saken (1988) detected a $\sim 1°$ diameter shell of infrared emission centered $\sim 30'$ eastward of the pulsar and concident with an H I shell (Koo et al. 1990). Both shells are almost circular with their southwestern portion open. The estimated dynamic age of the H1 shell of $9.6 \times 10^4 d_{2.5}$ agrees reasonably well with the spin-down age, 1.1×10^5 yr. This strongly suggests that it is the SNR shell associated with the birth of PSR 1951+32 $\sim 10^5$ yr ago.

In this paper we present data acquired with the High Resolution Imager (HRI) and the Position Sensitive Proportional Counter (PSPC) aboard the *ROSAT* X-ray observatory. The format of the paper is the following: in § 2, we describe the observations; § 3 contains the results of the spatial, spectral and temporal analyses. Finally, a discussion of the results is presented in § 4.

2. OBSERVATIONS

The field containing PSR 1951+32 and CTB 80 was observed with both the HRI and the PSPC at the focus of the X-ray telescope aboard *ROSAT*. In the case of both instruments PSR 1951+32 was in the center of the 2° diameter circular field of view. Detailed descriptions of the satellite, X-ray mirrors, and detectors can be found in Trümper (1983) and Pfeffermann et al. (1986).

The HRI observations took place on 1992 October 21 and 22 for an effective exposure of 9946 s. The ~2″ angular resolution of the HRI allowed a clear detection of the pulsar, the compact nebula, and an extended diffuse nebula. The J2000 source position of PSR 1951+32 was determined to be $\alpha = 19^h52^m57^s.97$, $\delta = 32°52'41''.3$. Given the known attitude uncertainties this is in good agreement with the adopted radio position (Cordes, Foster, & Weisberg 1992). The PSPC observations took place on 1991 April 5 and November 6 for effective exposures of 8318 and 552 s, respectively. The PSPC image shows also a hard conelike feature extending out to the detector edge. The data handling and analysis were performed with the MIDAS/Exsas software package.

3. RESULTS

3.1. *Spatial*

In the top panel of Figure 1 we display the shaded intensity map and contours of constant counts from the HRI X-ray image (white) superposed upon the 21 cm radio contours (black) of Angerhofer et al. (1981). A bright ~1′ radius compact core (dark filled circle) is clearly visible at the right of Figure 1, as well as a diffuse nebula extending ~5′ to the east. There is a strong correlation between the radio synchrotron plateau and the X-ray diffuse emission eastward of the pulsar. A close-up view of the 1′ radius compact core is displayed in the lower panel of Figure 1. This core contains a pointlike

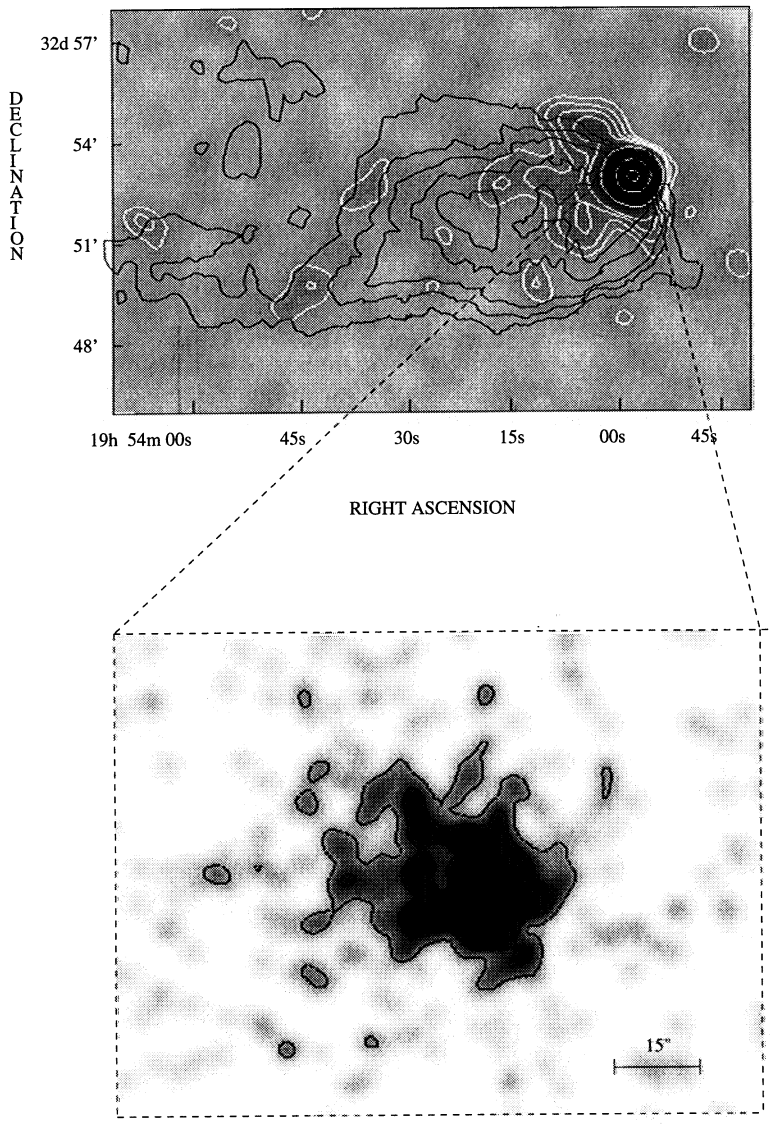

FIG. 1.—The HRI shaded intensity map and the contours of constant counts (white) superposed upon the 21 cm radio contours (black) (Angerhofer et al. 1981). The X-ray contours of 1.0, 1.1, 1.2, 1.3, 1.5, 2.0, 3.0, and 5.0 counts show the ~1′ radius compact core and the associated diffuse emission nebula extending ~5′ to the east (left) of the pulsar. The bottom panel is the bright 1′ compact core containing the point source (the pulsar) and the compact nebula offset 13″ from the pulsar.

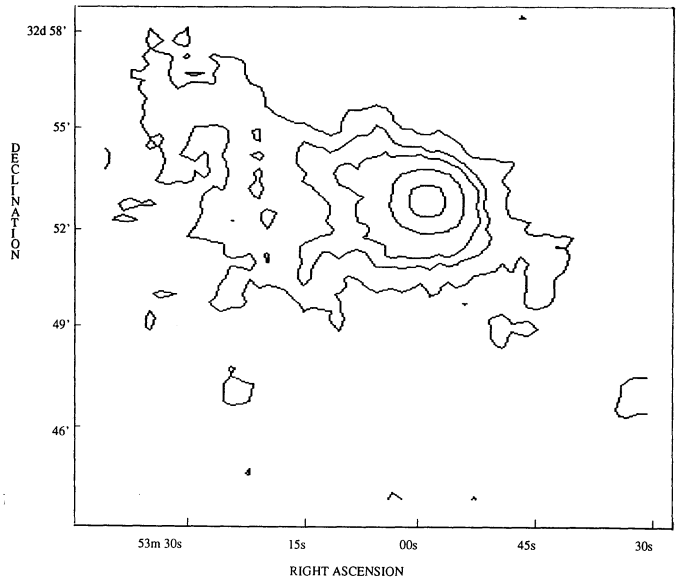

FIG. 2.—The constant X-ray surface brightness contours of the PSPC data revealing the plerionic component of CTB 80 in the 0.1–2.4 keV energy range. The map displays a circular compact core (~1′) and an extended diffuse nebula eastward of the pulsar out to ~8′. The contour levels (in units of 10^{-3} counts arcmin^{-2}) are 0.1, 0.15, 0.2, 0.5, 0.9, and 10. The image has been smoothed with a Gaussian with $\sigma = 72''$.

source (the pulsar) with a compact nebula offset from the pulsar by ~15″ and extending 35″ to the east. We also note that this core looks very similar to the radio core (Strom 1987).

In Figure 2 we display the constant surface brightness PSPC X-ray contours from the central region of CTB 80 in the 0.1–2.4 keV energy range. A Gaussian smoothing with $\sigma = 72''$ was applied to the data in Figure 2. The map shows the circular compact core (~1′ radius), and a diffuse emission region extending out to ~8′ east of the pulsar. The morphology (i.e., compact core and diffuse emission east of the pulsar) is the same as that observed with the HRI (see Fig. 1). However, owing to its higher sensitivity to diffuse emission with respect to the HRI, the PSPC image reveals a weaker emission region extending further out to ~8′. This morphology is also in agreement with the *Einstein* IPC map in that they both display the northeastern (NE) diffuse emission (referred to as "jetlike", in Wang & Seward 1984). However, we find no evidence for the southern lobe which appears in their map (Wang & Seward 1984).

In order to study the spectral characteristics of the pointlike source and the compact nebula, it is first necessary to separate the two components. To this end, we selected the photons contained within a ring of radius 250″ centered on the pulsar and subsequently performed a maximum likelihood fit to the observed radial count density profiles in six energy channels ranging from 0.1 to 2.4 keV. The deconvolution of the point source, compact nebula, and background incorporated the known point response function of *ROSAT*. The counts from the compact nebula were distributed with various radial nebular distribution functions determined iteratively. The background was taken as constant and determined in the region of the detector in close proximity to the compact nebula. The results of these fits were satisfactory and yielded the raw count rate distribution as a function of *ROSAT* energy channel. The point source counts (N_{ps}), compact nebula counts (N_{cn}), and background counts (B) are displayed in Table 1. The

TABLE 1

PSPC RESULTS FROM SEPARATING THE POINT SOURCE FROM THE COMPACT NEBULA WITH A MAXIMUM LIKELIHOOD METHOD

Energy Channel Band	N_{ps}	N_{cn}	B	χ^2/d.o.f.
10– 50	10	10	382	1.8
50– 80	63	102	245	1.1
80–110	190	210	149	1.4
110–140	160	185	123	2.3
140–170	100	115	109	1.0
170–240	80	60	49	1.1

NOTES.—The point source (N_{ps}), the compact nebula (N_{cn}), and the background (B) counts are indicated in six energy channels covering the 0.1–2.4 keV energy range of the PSPC and within a ring of 250″ centered on the pulsar.

scale size of the compact nebular radius was determined to be ~35″ containing half of the compact nebular counts. The total fitted and background subtracted point source and compact nebular count rates (within a radius of 250″) are 0.068 ± 0.003 and 0.077 ± 0.003 c s^{-1}, respectively. Our model indicates that half of the counts from the 1′ compact core originates in the point source, and the other half originates in the compact nebula.

3.2. *Spectral*

Utilizing the results of the deconvolution displayed in Table 1 we were able to study the spectral characteristics of the point source and the compact nebula separately. Due to its superior angular resolution we utilized the HRI map to determine the spatial extent of the diffuse nebula which is then used in the extraction of the PSPC events for spectral analysis. The spectra are best fit with a power-law representation, $dN/dE = KE^{-\Gamma}$, where Γ is the photon index, in the case of the point source, compact nebula, and diffuse emission. The photon index and the flux are sensitive to the interstellar column density range, N_H, which is not known accurately. Dispersion measure of the pulsar indicates a distance of ~1.5 kpc (Kulkarni et al. 1988; Fruchter et al. 1988). Kinematic estimates from the detected infrared shell indicate a distance close to 3 kpc (Fesen et al. 1988). The reddening $E(B-V) = 0.8$, derived from optical emission lines associated with the core of CTB 80, yields a distance close to 2.5 kpc (Blair et al. 1984; Hester & Kulkarni 1989; Angerhofer et al. 1980). In the following, we will express the distance d in units of 2.5 kpc. To determine the uncertainties in the fitted parameters we performed a χ^2 grid search of the interesting parameters. In Table 2 we summarize the 2 σ range of spectral parameters for the point-source, the compact nebula and the 5′ diffuse nebula at a fixed value of $N_H = 3.0$

TABLE 2

POWER-LAW MODEL RESULTS FOR THE POINT SOURCE, THE COMPACT NEBULA AND THE 5′ DIFFUSE NEBULA

Region	Γ	L_x (10^{33} ergs s^{-1})
Point source	$1.6^{+0.2}_{-0.2}$	2.3
Compact nebula	$2.1^{+0.2}_{-0.2}$	3.9
5′ Diffuse nebula	$1.8^{+0.5}_{-0.8}$	1.8

NOTES.—The photon index Γ (2 σ range) and the luminosity, L_x, are given for $N_H = 3.0 \times 10^{21}$ cm^{-2}. The distance was taken to be 2.5 kpc.

$\times 10^{21}$ cm^{-2}. The results corresponding to the full range of acceptable N_H values are discussed below. We also present the spectral fitting parameters of the hard emission from the conelike feature detected with the PSPC. The value of $N_H = 3.0 \times 10^{21}$ cm^{-2} was chosen because it represents the best-fitting value for the 1′ compact core, the 5′ diffuse nebula, as well as the conelike feature (see below).

3.2.1. *Point Source and Compact Nebula*

The point source spectrum is best described by the 2 σ range of the parameters $\Gamma = 1.0$–4.5, $N_H = (2.0$–$9.5) \times 10^{21}$ cm^{-2} while the compact nebular component is best described by the 2 σ range $\Gamma = 2.5$–5.5 and $N_H = (4.0$–$10.0) \times 10^{21}$ cm^{-2}. The compact nebula seems to have a softer spectrum than the point source. Table 2 indicates the spectral parameters at the fixed value of $N_H = 3.0 \times 10^{21}$ cm^{-2}, which will be adopted for the rest of the spectra (see below and § 4). We note that the N_H range is determined mainly by the point source and compact nebular counts in the soft band (channels 10–50). An increase of N_H by a factor of 2 (from 3.0×10^{21} cm^{-2} to 6.0×10^{21} cm^{-2} as was assumed in Wang & Seward 1984) increases the luminosities by a factor of ~ 10 and yields steeper spectra.

To check the above results we studied the spectrum of the entire 1′ core (containing both the point-source and the compact nebula). The corresponding spectrum was also best fit with a power law with 2 σ range of the parameters $\Gamma = 1.0$–3.2 and $N_H = (1.0$–$5.5) \times 10^{21}$ cm^{-2}. The N_H range, as expected, is narrower in this case since there are a larger number of counts in the soft band. The best-fitting value of N_H was 3.0×10^{21} cm^{-2}. This yields a 2 σ range for Γ of $2.1^{+0.2}_{-0.4}$ and a corresponding X-ray luminosity of $L_x = 5.4^{+1.1}_{-1.3} \times 10^{33} d^2_{2.5}$ ergs s^{-1} in the 0.1–2.4 keV band. The latter value of Γ agrees, within the errors, with the average value of 1.9 that we get from fitting of the point-source and compact nebula separately at the same value of N_H (see Table 2). Also, knowing that the 1′ ring includes the point source counts and $\sim 80\%$ of the compact nebular counts, the total luminosity of 5.4×10^{33} ergs s^{-1} is bracketed well by the fitted value above.

3.2.2. *The 5′ Diffuse Nebula*

The 5′ diffuse emission region is also best fit with a power law with 2 σ ranges of the parameters $\Gamma = 1.0$–3.7 and $N_H = (1.0$–$7.5) \times 10^{21}$ cm^{-2}. The best-fitting value of N_H was again 3.0×10^{21} cm^{-2}. The corresponding 2 σ range of the photon index is $\Gamma = 1.8^{+0.5}_{-0.8}$ with a luminosity of $L_x = 1.8 \times 10^{33} d^2_{2.5}$ ergs s^{-1} in the 0.1–2.4 keV band (see Table 2). The power-law model describes the eastward diffuse feature out to $\sim 8'$ with a slight (but not significant) decrease in the photon index. In addition, thermal plasma models do not yield satisfactory fits to the spectrum and, therefore, rule out a thermal nature for the diffuse emission. This data is then consistent with a synchrotron mechanism giving rise to the diffuse nebula, an interpretation which is in agreement with the observed nonthermal nature of the radio plateau (Angerhofer et al. 1981).

3.2.3. *The Conelike Feature*

In Figure 3 we display the PSPC image of CTB 80 for the full 2° diameter circular field of view in a hard (1.0–2.4 keV) band. The soft band (0.1–0.5 keV) image is featureless, while the medium band (0.5–1.0 keV) and hard-band images show a conelike feature in the southeast quadrant of the detector. To avoid confusion with the compact core and the extended diffuse nebula the counts from this conelike feature were extracted from the region of the detector extending from 8′ to 40′ SE of the position of the pulsar. The corresponding spectrum is well described by a two-temperature Raymond-Smith thermal plasma (Raymond & Smith 1977) model with temperatures of $kT_1 = (0.2$–$0.3)$ keV and $kT_2 = (0.8$–$1.5)$ keV and emission measures, derived from the normalization constant $K = \mathrm{EM}/4\pi D^2$, of $\mathrm{EM}_1 = (0.8$–$6.0) \times 10^{56}$ cm^{-3} and $\mathrm{EM}_2 = (0.8$–$1.5) \times 10^{56}$ cm^{-3}, respectively (2 σ ranges). The best-fitting average temperature is $\sim 1.0^{+0.6}_{-0.3} \times 10^7$ K (2 σ) and corresponds to a luminosity of $\sim 1.0 \times 10^{34} d^2_{2.5}$ ergs s^{-1}. The corresponding best-fit value of N_H is 3.0×10^{21} cm^{-2} and the reduced χ^2 is 0.8 for 15 d.o.f. We also did a χ^2 grid of the emission measure versus the temperature using the one-temperature component Raymond-Smith thermal plasma model, by allowing N_H to span a free range of reasonable values. The corresponding model parameters span a wide range of values, with the temperature $kT = (0.25$–$0.55)$ keV and the emission measure $\mathrm{EM} = (2.3$–$38) \times 10^{56}$ cm^{-3} (1 σ ranges). The corresponding luminosity is $(8.0 \times 10^{33}$–$1.1 \times 10^{35}) d^2_{2.5}$ ergs s^{-1}. The best-fitting temperature is $\sim 5.6 \times 10^6$ K, with an emission measure of $\mathrm{EM} = 4.0 \times 10^{56}$ cm^{-3} and corresponds to a luminosity of $\sim 1.2 \times 10^{34} d^2_{2.5}$ ergs s^{-1}. The corresponding best fit of N_H is 7.0×10^{21} cm^{-2} and the reduced χ^2 is 1.2 for 17 d.o.f. We note that the cooling function is constant over this wide range of values and is equal to $\Lambda \sim (3.0$–$4.0) \times 10^{-23}$ ergs cm^3 s^{-1}.

A power law yields an adequate fit with again a best fitting N_H of 3.0×10^{21} cm^{-2} and a corresponding luminosity of $\sim 2.0 \times 10^{35} d^2_{2.5}$ ergs s^{-1}. However, the photon index was very steep ($\Gamma \geq 4$).

3.3. *Temporal*

We used both the PSPC and the HRI data to test for pulsations at the radio period. For the PSPC we used an extraction radius of 80″ yielding 1040 counts in all energy channels. From the spatial analysis discussed previously, we estimate that $(45 \pm 6)\%$ of these extracted counts are from the pointlike source and the rest are from the compact nebula and background. For the HRI we used an extraction radius of 7.″5 yielding 226 counts where $\sim 75\%$ are from the point souce. The arrival times of the photons were reduced to the solar system barycenter using the JPL DE200 ephemeris and the J2000 coordinates listed in Table 3. Subsequently, we determined the arrival phases of the PSPC photons using the PSR 1951+32 radio ephemeris (Cordes et al. 1992) from GRO/radio timing data base. For the HRI photons, which were outside of the valid range of the above timing base, we used the most recent ephemeris from Foster et al. (1993). For both data sets the frequency f and its derivatives $\dot{f}$ and $\ddot{f}$ were known to a sufficient accuracy such that each X-ray photon could be directly phase related to the radio pulse with an absolute accuracy of 0.1 phases; the relative accuracy for the duration of each observation is better. The pulsar parameters used in the pulsar phase determination are listed in Table 3. The resulting pulse shapes are displayed in Figure 4. Both the PSPC and HRI pulses in the figure show a peak of width 0.1–0.2 phases, approximately in phase with the radio phase. The Z^2_n statistic test (Buccheri et al. 1993) was then calculated for the PSPC and the HRI data:

$$Z^2_n \equiv \frac{2}{N} \sum_{k=1}^{n} \left[\left(\sum_{i=1}^{N} \cos 2\pi k \phi_i \right)^2 + \left(\sum_{i=1}^{N} \sin 2\pi k \phi_i \right)^2 \right]$$

(ϕ_i is the residual phase of the ith event, and N is the total number of events). The main advantage of this test is that it is

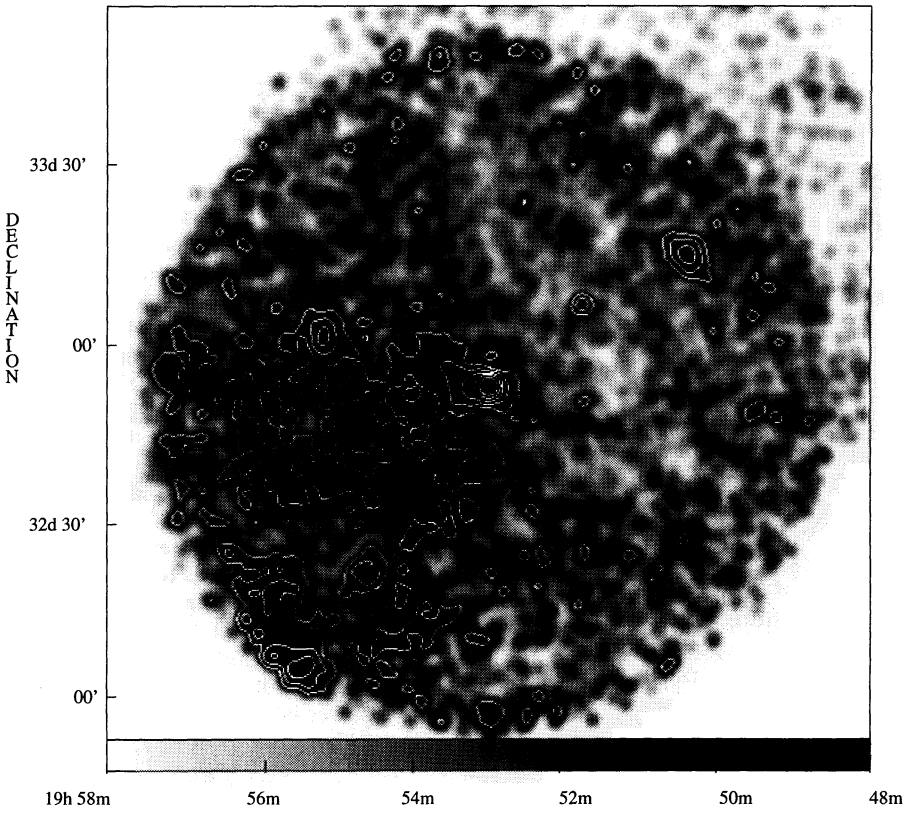

FIG. 3.—The dead-time corrected and vignetting-corrected PSPC image of CTB 80 in the hard (1.0–2.4 keV) band corresponding to an effective exposure of ~9 ks. The pulsar is at the center of the 2° diameter circular field of view. The PSPC image is featureless in the soft band while in the hard and medium (not shown) bands, the SE conelike feature is clearly evident.

independent of binning and the increase of the significance of Z_n^2 as a function of n, the number of summed harmonics, indicates the harmonic content of the pulse shape; for a random set of arrival phases Z_n^2 should be distributed like χ^2 with $2n$ d.o.f. In the case of the PSPC data Z_n^2 keeps on increasing in significance up to $n = 6$ where it reaches a confidence level of 98.2%; the high harmonic content (i.e., the low-duty cycle) is also evident from the PSPC pulse shape in Figure 4. In the case of the 226 HRI photons, the statistics are too poor to detect a very significant signal even at the first harmonic ($Z_1^2 = 3.46$, confidence level 82%). Combining the PSPC and HRI in absolute phase increases the confidence level for detection of pulsations at the radio period to ~99%. The implied pulsed fraction of the analyzed PSPC photons is $16 \pm 3\%$; when we consider that only 45% of the analyzed photons are from the pulsar, we get 35% as the pulsed fraction of the photons emanating from the point-source, i.e., the pulsar.

It has been recently observed that a number of X-ray emitting rotation-powered neutron stars have energy-dependent pulse shapes (see Ögelman 1994 for a review). We examined the PSPC data of PSR 1951+32 for similar behavior by dividing the 1040 events into 10 energy channel intervals each having ~100 photons and investigating the pulse shape changes. Although 100 photons are not sufficient to deliniate a pulse shape it is possible to recognize general trends like phases of the first harmonic and pulsed fractions. Figure 4 shows the phase of the first harmonic Z_1^2, the value of the Z_1^2 statistic, and the value of the Z_6^2 statistic as a function of the energy-channel. Several interesting features emerge in Figure 5. One is the trend of the peak of the first harmonic to move to earlier phases as the energy of the photons gets higher, or within uncertainties, a complicated energy dependent behavior. The second is the peaked behavior of the Z_1^2, the power in the first harmonic, as if most of the pulsed photons have energies around 1.3 keV

TABLE 3

SUMMARY OF RADIO PULSAR DATA USED IN THE PULSATION ANALYSIS OF THE POINT SOURCE

Date	Epoch[a] (TDB JD)	ν_0 (Hz)	$\dot{\nu}$ (Hz s^{-1})
1991 Apr 5–6, Nov 26 (PSPC).....	2,448,352.352037355	25.296961875	-3.745×10^{-12}
1992 Oct 21–22 (HRI)	2,448,917.203345116	25.296779295	-3.741×10^{-12}

[a] The epoch is also the radio arrival time at the solar system barycenter in the Barycentric Dynamical Time (TDB) scale.

NOTE.—The J2000 coordinates used for the PSPC data and HRI data are, respectively, $\alpha = 19^h52^m58^s.322$, $\delta = +32°52'41''.88$ and $\alpha = 19^h52^m58^s.298$, $\delta = +32°52'40''.48$.

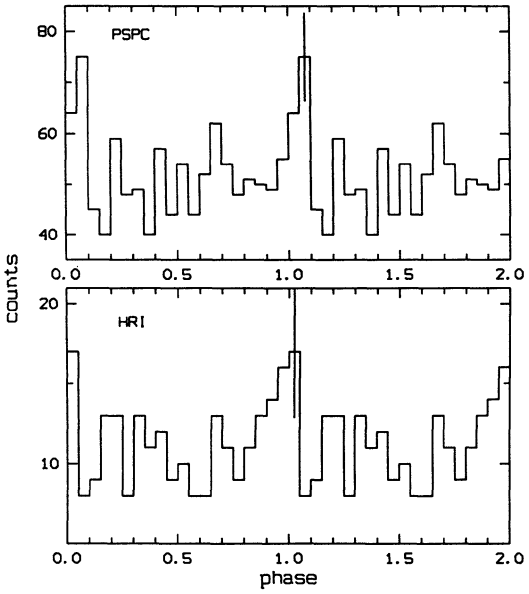

FIG. 4.—The pulse shapes of the PSPC and the HRI data of PSR 1951+32 with the parameters listed in Table 4.

(pulsed fraction of the power in first harmonic $\simeq[(2/100)(Z_1^2 - 2)]^{1/2}$. The third is the structure in the Z_6^2, the total power in the first six harmonics, which shows a peak at the lowest energies around 0.1 keV, and another one around 1.3 keV (pulsed fraction of the power in the first six harmonics $\simeq[(2/100)(Z_6^2 - 12)]^{1/2}$).

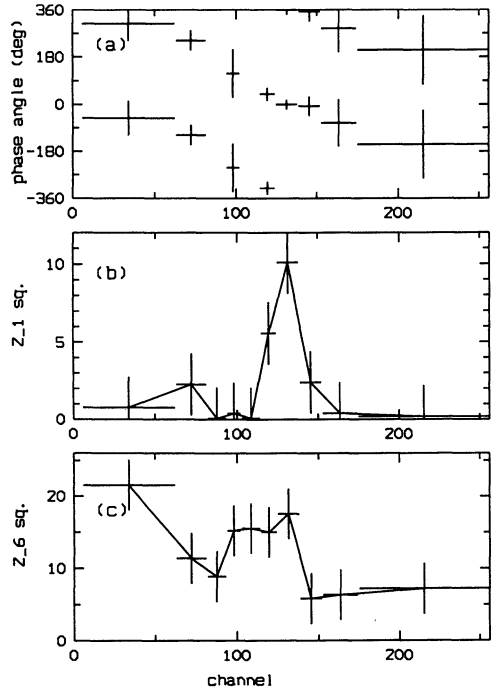

FIG. 5.—The phase of the first harmonic (the phase angle information has been repeated modulo 360°); (*top*) the first harmonic poer Z_1^2; (*middle*) the power in the total of the first six harmonics Z_6^2; (*bottom*) as a function of pulse height channel. The energy in keV is approximately the channel number divided by 100. The phase angle is with respect to the main peak of the radio pulse.

4. DISCUSSION

ROSAT HRI and PSPC observations of the SNR CTB 80 containing the pulsar PSR 1951+32 have been reported. The observed X-ray morphology comprises three distinct regions: The bright 1′ compact core (point-source and compact nebula), the diffuse ~8′ nebula and the conelike feature SE of the pulsar. Power-law models gave adequate fits to the compact core and the diffuse extended nebula suggesting synchrotron emission.

4.1. *The Pulsar and Compact Nebula (Compact Core)*

The 39.5 ms pulsar which gives the plerionic character to CTB 80 is an unusual pulsar in the sense that it has the lowest magnetic field among its contemporaries, $B = 4.9 \times 10^{11}$ G. The short spin period still makes it the fifth largest in spin-down energy-loss rate $\dot{E} = 3.7 \times 10^{36}$ ergs s^{-1}, after the Vela pulsar. The X-ray luminosity of the pulsar in the 0.1–2.4 keV band of *ROSAT* is $\sim 2.3 \times 10^{33}$ ergs s^{-1} (at 2.5 kpc), which is about a factor 1.7 smaller than that predicted from the period and surface magnetic field values with the empirical magnetospheric luminosity model of Ögelman (1994). Essentially, the magnetospheric luminosity appears to be capable in accounting for the observed X-ray luminosity from the pulsar, and it would not be possible to observe the $\sim 10^{33}$ ergs s^{-1} cooling luminosity expected from a neutron star of 10^5 yr age.

The total X-ray luminosity radiated by the pulsar, the compact nebula and the diffuse emission represents only $\geq 0.2\%$ of $\dot{E}$. Hence PSR 1951+32, like other pulsars, must be losing most of its rotational energy via a relativistic wind consisting of particles and field. Confinement of the pulsar wind can arise in a spatially extended region emitting X-rays by synchrotron radiation. If, as suggested, PSR 1951+32 was born at the center of the SNR shell detected in H I (Koo et al. 1990) and infrared emission (Fesen et al. 1988) the pulsar should presently be encountering the western edge of the SNR shell. It is this SNR shell or possibly a nearby cloud (from the optical observations; Hester & Kulkarni 1988) which is the source of confinement of the pulsar wind. The condition for confinement is $\rho v_p^2 > P_T$, where ρ is the mass density of the medium, v_p is the velocity of the pulsar through the ambient ISM and P_T is the total pressure of the synchrotron nebula. Since the pulsar velocity is relatively high (300–500 km s^{-1}; Kulkarni et al. 1988, Strom 1987), a modest density of a few amu cm^{-3} would be enough to confine the pulsar wind. Confinement of the wind can result in a strong reverse shock to be driven back into the wind. This heating of the plasma by this reverse shock can result in emission by synchrotron processes far outside the light cylinder (Cheng 1983). The shock radius is given by

$$\frac{\Omega r_s}{c} = 1.7 \times 10^5 I_{45}^{1/2} P^{-5/2} \dot{P}_{-15}^{1/2} v_7^{-1} \rho^{-1/2} \; ; \qquad (1)$$

which yields $r_s \sim 8.0 \times 10^{16}$ cm (~ 0.026 pc) and an angular size of $\sim 2''$ at 2.5 kpc (assuming a density of 1 amu/cm^{-3}). This distance is reasonable since it coincides with the hot spot detected SW of the pulsar (Strom 1987), and strengthens the argument that the hot spot is a Crab-like wisp where the pulsar wind is shocked and where the nebular region starts. However, such a feature cannot be resolved with *ROSAT*. Assuming a power-law distribution of electrons with an index γ, the observed photon index of $\Gamma \sim 2$ (see Table 2) for $N_H = 3 \times 10^{21}$ cm^{-2}, corresponds to $\gamma = 3$ (like the Crab). The corre-

sponding extended flux density is (Cheng 1983)

$$F_x^e = 0.4 \times 10^{-26}\left(\frac{\text{keV}}{h\nu}\right)\xi \frac{\sigma^{3/4}}{(1+\sigma)^{3/4}} \text{ ergs cm}^{-2}\text{ s}^{-1}\text{ Hz}^{-1}\ ; \quad (2)$$

where σ is the ratio of the poynting flux to the particle flux, and ξ is the fraction of the plasma density accounted for by the radiating charges. For the energy range of 0.1–2.4 keV we calculate the integrated X-ray flux to be $3 \times 10^{-9}\ \sigma^{3/4}/[(1+\sigma)^{3/4}]\xi$ ergs cm^{-2} s^{-1}. The corresponding luminosity is $\sim 2.4 \times 10^{36}\xi\sigma^{3/4}/[(1+\sigma)^{3/4}]$ ergs s^{-1}. For small σ, the condition that $\xi < 1$ puts a lower limit on σ of $\geq 3 \times 10^{-4}$ for $N_H = 3 \times 10^{21}$ cm^{-2} or $\sigma \geq 1 \times 10^{-2}$ for $N_H = 6 \times 10^{21}$ cm^{-2}.

4.2. *The Diffuse Eastern Nebula*

To estimate the magnetic field in the diffuse nebula, we assume the diffuse emission region to be a cylinder extending to the NE of the position of the pulsar from 1′ to 5′ and of diameter 5′. The corresponding volume of this region is then $\sim 1.0 \times 10^{57}$ cm^3. We use the value $\Gamma \sim 1.8$ and note that the magnetic field calculation is insensitive to the uncertainties in Γ arising from different valus of N_H. Assuming a synchrotron model and equipartition between particle and energy density, we calculate the magnetic field in the diffuse nebula to be $\sim 3.4 \times 10^{-6}$ G. The corresponding average Lorentz factor of the electrons is therefore $\sim 1.6 \times 10^8$, implying relativistic electrons with a lifetime of $\sim 20{,}000$ yr.

The morphology of the diffuse eastern nebula can be explained in the following way. Once the shocked pulsar wind emerges from the reverse shock, it forms the compact core. However, the high ram pressure encountered by the pulsar (probably moving in the westward direction as suggested by the HRI picture and by Fesen et al. 1988) and possibly the pressure gradient between the pulsar nebula and the medium swept out by the pulsar in its motion causes the plasma to be blown further out behind the pulsar (i.e., in the eastward direction). We note that this coincides well with the magnetic field structure in the radio plateau as derived from polarization measurements by Angerhofer et al. (1981). This scenario can explain the eastward extent of the synchrotron plateau as well as the sharp edges seen in the diffuse emission feature to the NE and SW. However, the asymmetry in this feature may arise from an asymmetry in the medium that the pulsar encounters. The possible presence of a cloud SW of the pulsar as suggested by Hester & Kulkarni (1988), the detection of a hot spot in this region indicative of highly shocked material (Strom 1987), and our HRI image all seem to be in agreement.

4.3. *The Conelike Feature*

The cone-like feature overlaps the eastern radio ridge and is mainly concentrated at the detected H I and infrared shell. Fesen et al. (1988) suggested that the radio emission in the outer ridges of CTB 80 result from synchrotron radiation along the compressed magnetic field in the SNR shell. In Figure 6 we display the strong correlation between this open shell in the SW, the radio morphology and the X-ray morphology of the thermal hot gas SE of the pulsar. However, we do not observe hard X-rays along the NE radio ridge, suggesting the existence of dense regions screening the hard X-rays.

Using the parameters derived from our thermal plasma fits (the two-temperature component fit), we calculate a thermal energy of $\sim 5 \times 10^{49}$ ergs. This represents $\sim 7\%$ of the explo-

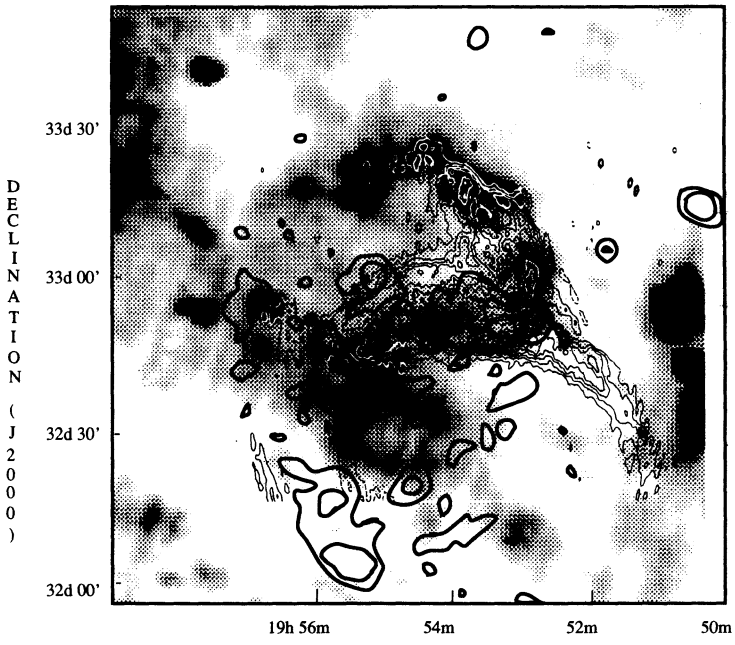

FIG. 6.—The X-ray contours of CTB 80 in the (1.0–2.4) keV hard band (*dark contours*) superposed upon the brightness distribution of the 49 cm radio ridges (*light contours*), and the 1° diameter shell of infrared emission (*shaded regions*; Koo et al. 1993). The pulsar, embedded in the bright core, is located at the western edge of the remnant. The synchrotron X-ray emission overlaps the nonthermal radio plateau (10′ × 6′). The conelike feature extends SE of the pulsar and is concentrated at the eastern radio ridge and the SE portion of the IR shell.

sion energy of the supernova as estimated by Koo et al. (1990). By normalizing the X-ray emitting region to the total volume of the SNR shell (assuming a complete shell of radius $\sim 24 d_{2.5}$ pc) this fraction can go up to 26%. The average electron density is $n_e \sim 0.02$ cm^{-3} (from the emission measure), implying a hot, low-density medium. The thermal pressure ($P = 2n_e kT$) is $\sim 4.0 \times 10^{-11}$ dynes cm^{-2}, which represents ~ 10 times the average diffuse ISM density. Taking into consideration the dynamic age of the detected H I shell of $\sim 9.6 \times 10^4 d_{2.5}$ years and its expansion velocity of ~ 70 km s^{-1} (Koo et al. 1990, after normalizing their values to a distance of 2.5 kpc), the above results as well as the derived value of the cooling function (previous section) are consistent with thermal emission from a SNR in its radiative cooling phase (Cox 1972; McKee & Ostriker 1977; Mansfield & Salpeter 1974; Falle 1975). We note that a power-law model yields a satisfactory fit and cannot be ruled out. However, the photon index is very steep ($\Gamma \geq 4$). If the synchrotron emitting electrons in the cone-like emission region were to have the remnant's age of $\sim 10^5$ yr, then they must be very energetic. We consider this highly unlikely given the adiabatic losses.

In conclusion, CTB 80 represents a composite-type SNR whose unique morphology results from the activity of a fast-spinning pulsar encountering the edge of an old SNR. PSR 1951+32 represents a relatively old pulsar, but its large "Vela-like" rotational energy loss ($\dot{E} = 4 \times 10^{36}$ ergs s^{-1}) arising from its fast period powers a synchrotron nebula (the plerionic component), as well as rejuvenates an old SNR by the injection of relativistic particles (the shell-like component). However, the X-rays detected out to the infrared shell imply a very hot gas cooling in a very low density medium. This would be unlikely for old remnants. A measurement of the pulsar's proper motion and a better handle on the ambient ISM density are needed before a better understanding of the X-ray morphology and its relation to the radio ridges in CTB 80 will be possible.

We thank D. Cox, R. Edgar, W. Kluźniak, W. Kundt, and J. Shaham for illuminating discussions and D. Backer and R. Foster for helping with the pulsar timing ephemeris. This research was supported by NASA grant NAGW-2643.

REFERENCES

Angelini, L., White, N. E., Parmar, A. N., Smith, A., & Stevens, M. A. 1988, ApJ, 330, L43
Angerhofer, P. E., Strom, R. G., Velusamy, T., & Kundu, M. R. 1981, A&A, 94, 313
Angerhofer, P. E., Wilson, A. S., & Mould, J. R. 1980, ApJ, 236, 143.
Blair, W. P., Kirshner, R. P., Fesen, R. A., & Gull, T. R. 1984, ApJ, 282, 161
Buccheri, R., et al. 1983, A&A, 128. 245
Cheng, A. F. 1983, ApJ, 275, 790
Cordes, J. M., Foster, R. S., & Weisberg, J. M. 1992, *GRO*/radio timing data base, Princeton Univ.
Cox, D. P. 1972, ApJ, 178, 159
Falle, S. A. E. G. 1975, MNRAS, 172, 55
Fesen, R. A., Shull, J. M., & Saken, J. M. 1988, Nature, 334, 229
Foster, R. S., Lyne, A. G., Shemar, S., & Backer, D. C. 1993, preprint
Fruchter, A. S., Taylor, J. H., Backer, D. C., Clifton, T. R., Foster, R. S., & Wolszczan, A. 1988, Nature, 331, 53
Hester, J. J., & Kulkarni, S. R. 1988, ApJ, 331, L121
———. 1989, ApJ, 340, 362
Koo, B., Reach, W. T., Heiles, C., Fesen, R. A., & Shull, J. M. 1990, ApJ, 346, 178
Koo, B., Yun, M., Ho, P. T., & Lee, Y. 1993, ApJ, 417, 196
Kulkarni, T., Clifton, T. R., Backer, D. C., Foster, R. S., Fruchter, A. S., & Taylor, J. H. 1988, Nature, 331, 50
Mansfield, V. N., & Salpeter, E. E. 1974, ApJ, 190, 305
Mantovani, F., Reich, W., Salter, C. J., & Tomasi, P. 1985, A&A, 145, 50
McKee, C. F., & Ostriker, J. P. 1977, ApJ, 218, 148
Ögelman, H. 1994, in Proc. NATO ASI on the Lives of Neutron Stars, ed. A. Alpar, Ü. Kiziloğlu, & J. van Paradijs (Dordrecht: Kluwer)
Ögelman, H., & Buccheri, R. 1987, A&A, 186, L17
Pfeffermann, E., et al. 1986, Spie, 733, 519
Raymond, J. C., & Smith, B. W. 1977, ApJS, 35, 419
Strom, R. G. 1987, ApJ, 319, L103
Strom, R. G., Angerhofer, P. E., & Dickel, J. R. 1984, A&A, 139, 43
Trümper, J. 1983, Adv. Space Res., 2, 241
Velusamy, T., & Kundu, M. R. 1974, A&A, 32, 375
Velusamy, T., Kundu, M. R., & Becker, R. H. 1976, A&A, 51, 21
Wang, Z. R., & Seward, F. D. 1984, ApJ, 285, 607
Weiler, K. W. 1985, in The Crab Nebula and Related Supernova Remnants, ed. M. Kafatos & R. B. C. Henry (Cambridge Univ. Press), 227
Whitehead, M. J., Meaburn, J., & Clayton, C. A. 1989, MNRAS, 237, 1109